J Mater Sci: Mater Electron (2011) 22:872–875
DOI 10.1007/s10854-010-0228-2

The change in the electrical transport mechanism from the grain boundary conduction to the nearest-neighbor hopping conduction in SnO_2

A. Yildiz · A. A. Alsaç · T. Serin · N. Serin

Received: 29 July 2010 / Accepted: 29 September 2010 / Published online: 10 October 2010

Abstract The electrical conductivity measurements on SnO_2 over a wide range of temperatures were performed. The results provided experimental evidence for a transition from the grain boundary (GB) conduction at high temperatures to the nearest-neighbor hopping (NNH) conduction at low temperatures. In the light of employed conduction models, characteristic parameters describing the electrical transport in SnO_2, such as the grain barrier height and donor concentration were determined. Atomic force microscopy (AFM) and X-ray diffraction (XRD) measurements of SnO_2 were also presented.

1 Introduction

Tin dioxide (SnO_2) has received considerable interest in scientific research because of the potential technological applications such as gas sensors and solar cells [1, 2]. It is an n-type metallic oxide, wide band-gap semiconductor (E_g = 3.6 eV). Understanding the electrical conduction mechanism of SnO_2 is condition required in its device applications. In spite of the fact that a number of studies are available on SnO_2 thin films still there is a lot of scope to investigate on the electrical conduction mechanism in SnO_2.

Since polycrystalline materials are consist of small crystallites joined at their surfaces via grain boundaries (GBs), the high temperature conductivity of polycrystalline materials is related to the potential barriers built up around the GBs [3, 4]. The presence of imperfections leads to the occurrence of the localized states in the band gap in polycrystalline materials. In such a case, the carriers do not have sufficient energy to cross the potential barrier and then conduction takes place through hopping between the localized states at low temperatures. On the other hand, it is possible to observe hopping conduction at even about room temperature in SnO_2 due to high E_g and small Bohr radius (a_B*) [5–7].

There are two main types of hopping; variable-range hopping (VRH) and nearest-neighbor hopping (NNH) [8]. As the temperature decreases, the electrons have not sufficient energy to cross the potential barrier in n-type material. In this case, the GB conduction becomes less important. In the NNH conduction, electron with an activation energy hops to the nearest neighboring empty site. This activation energy has much smaller value as compared to the energy required for the GB conduction. According to Mott [8], electron hopping between nearest neighbor sites is not always favored at low temperatures as the levels may be significantly different in energy. It is possible that electrons can prefer to move to a more energetically similar remote site. This type conduction is known as the VRH.

To the best of our knowledge, no work providing a detailed explanation for the crossover from the GB to the NNH in SnO_2 as temperature decreases has been presented to date. In this work, we present that there is a clear crossover between the GB conduction and the NNH conduction in SnO_2.

2 Experimental

The 1 mm thick rectangular shaped (26 × 76 mm^2) glass substrates were ultrasonically cleaned in de-ionized water

A. Yildiz (✉)
Department of Physics, Faculty of Science and Arts,
Ahi Evran University, 40040 Kirsehir, Turkey
e-mail: yildizab@gmail.com

A. A. Alsaç · T. Serin · N. Serin
Department of Engineering Physics, Faculty of Engineering,
Ankara University, 06100 Ankara, Turkey

and acetone (CH_3COCH_3, Merck) for 30 min. They were dried in the furnace 100°C at for 10 min. The SnO_2 solution was obtained by means of dissolving 8.37 g of stannous chloride $SnC1_22H_2O$ in 100 ml of absolute ethanol [C_2H_6O, Merck]. The solution was stirred and heated in a closed vessel. Then the vessel was opened, and the solution again stirred and heated until the solvents were completely evaporated. Finally, powders were obtained. Then, powders were dissolved in 50 ml of absolute ethanol. The solution was finally stirred and heated at 50°C for 2 h. The cleaned glass substrates were dipped into the solution and withdrawn at a constant speed of 80 mm min^{-1}. Each coating on glass substrate was heated at 500°C for 10 min in the furnace. This process coating was repeated to get the desired film thickness. The thickness of investigated film was obtained as 351 nm by means of optical transmission spectrum using the envelope method [9].

The microstructure of the deposited films was investigated by means of an Inel-EQUINOX 1000 diffractometer. The radiation source, wavelength, and scanning range 2 h of the diffractometer were Co K_α, 0.179 nm, and 15 ° to 70 °, respectively.

The electrical conductivity measurements were carried out using Keithley 2420 programmable constant current source in a temperature range of 210–350 K. The surface morphology of the films was also observed by a SPM Solver-PRO (NT-MDT) in semi-contact mode. The root mean square (RMS) values of surface roughness were estimated.

3 Results and discussion

The X-ray diffraction patterns of studied films are shown in Fig. 1. It is clear that film deposited is SnO_2 of polycrystalline in nature. A matching of the observed and the standard (hkl) planes confirm that the deposited film is of SnO_2 having primitive tetragonal structure [10]. Since the peak intensities almost the same for all direction it can be said that no significant preferential growth in any direction exists. The lattice constants a and c for the tetragonal phase structure are determined by the relation,

$$\frac{1}{d^2} = \left(\frac{h^2}{a^2} + \frac{k^2}{a^2}\right) + \left(\frac{l^2}{c^2}\right) \quad (1)$$

where d and (hkl) are the inter planer distance and miller indices, respectively. The lattice constants a and c are calculated as 0.497 and 0.329, respectively. It was observed that lattice constants calculated match well with the standard JCPDS data card [10].

The size of the crystallites (L) oriented along (101) plane is determined using Scherrer's formula [11]

$$L = \frac{0.9\lambda}{B\cos\theta} \quad (2)$$

where B, θ and λ are the broadening of diffraction line measured at half its maximum intensity in radians, the diffraction angle and the X-ray wavelength, respectively. The calculated value of crystallite size is 5.1 nm.

The surface morphology of the film is shown in Fig. 2. AFM analysis showed that film is polycrystalline and has the needle-shaped of nano grains. The root mean square

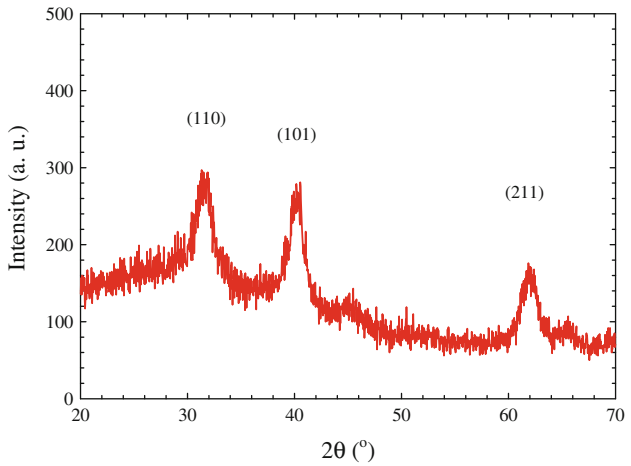

Fig. 1 XRD spectra of SnO_2

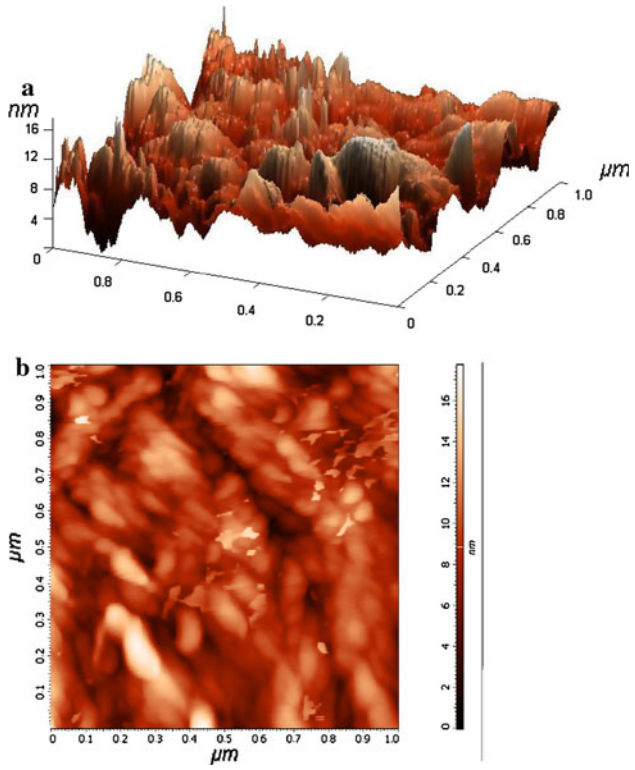

Fig. 2 **a** Three-dimensional (3D) and **b** two-dimensional (2D) AFM images for SnO_2

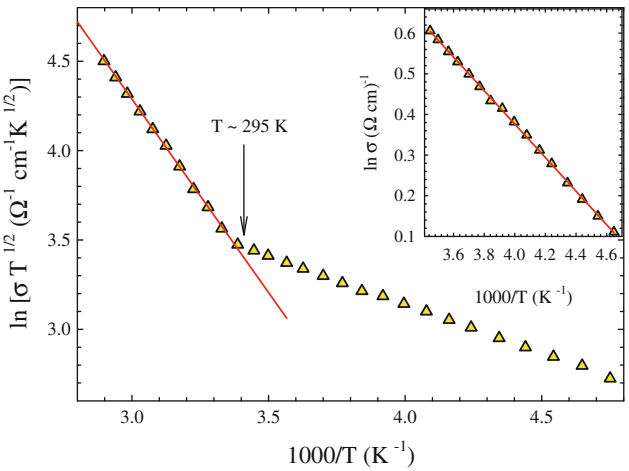

Fig. 3 Temperature dependence of the conductivity plotted as $\ln(\sigma T^{1/2})$ vs. $10^3/T$. *Solid lines* are the best-fit lines with Eq. (3). The inset of Fig. 3 represents the conductivity plotted as $\ln(\sigma)$ vs. $10^3/T$. *Solid lines* are the best-fit lines with Eq. (13)

(RMS) value of surface roughness and crystallite size were estimated as 2.51 and 53 nm, respectively. The large difference between sizes found from XRD and AFM could be explained by the formation of large grains from several sub-grains or crystallites.

Figure 3 shows the plot [$\ln(\sigma T^{1/2})$ vs. $10^3/T$] for the film. The plot suggests that there are two types of conduction mechanisms contributing to the conductivity in different temperature ranges. These two mechanisms can be distinguished experimentally by operating in appropriate temperature ranges. The conductivity is found to increase with the increase in temperature and the increase is observed to be very gradual and small for temperatures below about 295 K.

The high temperature slope of Fig. 3 is related the GB conduction. Since a polycrystalline film has crystallites joined at their surfaces via the GB, the boundaries between crystallites play an important role in determining the conductivity of polycrystalline film. In a polycrystalline material, the conductivity at high temperature range follows the expression [3];

$$\sigma = \left(\frac{Le^2 n v_c}{k_B T}\right) \exp\left(-\frac{E_b}{k_B T}\right), \tag{3}$$

$$v_c = \left(\frac{k_B T}{2\pi m^*}\right)^{1/2}, \tag{4}$$

$$E_b = \frac{L^2 e^2 N_d}{8\varepsilon}. \tag{5}$$

In Eqs. (3–5) the following notations were used; e, electron charge; k_B, Boltzmann's constant; m^*(=0.3 m_0) [12], effective mass of charge carriers; E_b, barrier energy at boundary; N_D, donor concentration; ε (=13.5) [13], low frequency dielectric constant.

Applicability of grain boundary model involves many grain boundaries. This effect is examined by evaluation of the L_D in comparison with the L. L_D is given as [4],

$$L_D = \sqrt{k_B T \varepsilon_0 \varepsilon / e^2 N_d}, \tag{6}$$

If $L_D < L/2$, potential barriers exist in the GB region due to interface trap states [4]. If, however, L_D is larger than $L/2$, the conduction band becomes flat without the potential barrier [4]. Then electrons are transported without the GB scattering.

From the slope of the linear fit of $\ln(\sigma T^{1/2})$ vs. $10^3/T$ for high temperature range, the E_b was determined as 184 meV. Knowing the values of L and ε, the value of N_D and L_D were calculated as 4.22×10^{19} cm^{-3} and 0.68 nm, respectively. The condition $L_D < L/2$ is fulfilled for the sample. Therefore, the approach of analyzing the data using the GB model for the thermal activation of conductivity is valid for the sample at high temperature range.

From the Fig. 3, one can see that the temperature dependence of conductivity deviates from the linearity for temperatures less than 295 K, above which the GB model is valid. One may expect that the NNH conduction mechanism should dominate at low temperatures. For n-type semiconductors, most of the free electrons are recaptured by the donors at low temperatures. Then the electrons have not sufficient energy to cross the potential barrier [8]. In this case, the GB conduction becomes less important, and electron hopping directly between donor states in the impurity band will bring the main contribution to the conduction mechanism [8]. The existence of the localized states for such a conduction process is a consequence of imperfections associated with polycrystalline films. In polycrystalline materials, the hopping conduction process exists in the grain boundaries at temperatures at which the carriers do not have sufficient energy to cross the potential barrier and to transfer themselves into the crystallite by the process of thermionic emission [14].

In order to apply the NNH model, the condition is $r/a_B^* > 1$ [15]. Here, r is the NNH distance, respectively. The a_B^* and r are given with relations;

$$a_B^* = \frac{4\pi\varepsilon_0\varepsilon\hbar^2}{m^* e^2} \tag{7}$$

and

$$r = \left(\frac{4\pi N_d}{3}\right)^{-1/3} \tag{8}$$

The ratio of r/a_B^* was found as 1.21 nm for the sample. The requirement for the NNH, $r/a_B^* > 1$ is clearly satisfied for the sample. The curve inset of Fig. 3 is linear for

temperature range of 210–295 K, which reconfirms that the NNH model is most suitable for explaining the conduction process for temperature range of 210–295 K. In the NNH conduction, electron hops to the nearest neighbor empty site. For the localized states with an energy separation W and the NNH distance r, the hopping probability can be written as [16]

$$P_{hop} = v_{ph} \exp(-2r/\xi - W/k_B T) \quad (9)$$

where v_{ph} is the phonon frequency associated with hopping process, and ξ is the localization length. The diffusion coefficient D_{hop} for hopping is given by [16].

$$D_{hop} = P_{hop} r^2/6 \quad (10)$$

Using the Einstein relation, the conductivity can be written as

$$\sigma = e^2 D_{hop} N(E_F) \quad (11)$$

Combining Eqs. 9–11, the temperature dependence of conductivity in the NNH regime is found as [16]

$$\sigma = \left[\frac{1}{6} N(E_F) v_{ph} e^2 r^2\right] \exp(-2r/\xi - W/k_B T) \quad (12)$$

$$\sigma = \sigma_3 \exp(-W/k_B T) \quad (13)$$

where $[N(E_F)]$ is the density of states and W is defined as the average energy needed to hop to the nearest neighbor at a distance r. From simple potential considerations W can be estimated using the following equation [17]

$$W = \frac{e^2 N_d^{1/3}}{4\pi\varepsilon} \quad (14)$$

The activation energy ($W = 37$ meV) was obtained by fitting the temperature dependence of conductivity data to the NNH mechanism (Eq. 13). Then, the value of N_d can be obtained as 4.17×10^{19} cm^{-3}, which is in excellent agreement with extracted value from the Eq. 5. Thus, one can expect that theoretical models which considered explaining the electrical transport in the sample are suitable. This also confirms that there is a clear transition from the GB conduction at high temperatures to the NNH conduction at low temperatures in the sample.

4 Conclusion

The electrical conductivity, atomic force microscopy (AFM) and X-ray diffraction (XRD) measurements on SnO_2 were performed. The different conduction mechanisms were distinguished by performing the conductivity curves as a function of the temperature. For high temperatures, the temperature-dependence of the conductivity was found to follow the GB model, while the NNH behavior was observed at lower temperatures. Consequently, in this work, we provided important information in order to deeper understand the conduction mechanisms which are still now the most important issues for the device applications of SnO_2.

Acknowledgments This work is supported by the State of Planning Organization of Turkey under Grant No. 2001K120590 and the Ankara University BAP under Project Number 2007-07-45-054. We would also like to thank Prof. Dr. Yusuf Kağan Kadıoğlu and Ms. Murat Yavuz for providing XRD and AFM measurements.

References

1. G. Zhang, M. Liu, Sens. Actuators B: Chem. **69**, 144 (2000)
2. N. Barsan, U. Weimar, J. Phys.: Condens. Matter **15**, R813 (2003)
3. J.Y.W. Seto, J. Appl. Phys. **46**, 5247 (1975)
4. J.W. Orton, M.J. Powel, Rep. Prog. Phys. **43**, 1263 (1980)
5. A.J.C. Lanfredi, R.R. Geraldes, O.M. Berengue, E.R. Leite, A.J. Chiquito, J. Appl. Phys. **105**, 023708 (2009)
6. A. Yildiz, S.B. Lisesivdin, M. Kasap, D. Mardare, J. Non-Cryst. Solids **354**, 4944 (2008)
7. T. Serin, A. Yildiz, N. Serin, N. Yıldırım, F. Özyurt, M. Kasap, J. Electron. Mater. **39**, 1152 (2010)
8. N.F. Mott, E.A. Davis, *Electronic Process in Non-Crystalline Materials* (Clarendon, Oxford, 1979)
9. R. Swanepoel, J. Phys. E Sci. Instrum. **16**, 1214 (1983)
10. JCPDS Card no 41-1445 (Tetragonal SnO_2)
11. B.D. Cullity, *Elements of X-Ray Diffraction* (Addison-Wesley, Reading, MA, 1978)
12. T.J. Coutts, D.L. Young, X. Li, MRS Bull. **25**, 58 (2000)
13. R. Summit, J. Appl. Phys. **39**, 3762 (1968)
14. A. Yildiz, N. Serin, M. Kasap, T. Serin, D. Mardare, J. Alloy. Comp. **493**, 227 (2010)
15. A. Yildiz, N. Serin, T. Serin, M. Kasap, Jpn. J. Appl. Phys. **48**, 111203 (2009)
16. R.A. Street, *Hydrogenated Amorphous Silicon* (Cambridge University Press, Cambridge, 1991)
17. B.I. Shklovskii, Sov. Phys. Semicond. **6**, 1053 (1973)